ACS APPLIED MATERIALS & INTERFACES

www.acsami.org

Research Article

Semiconducting Polymer Interfaces for Electrochemically Assisted Mercury Remediation

Riccardo Candeago,[‖] Kwiyong Kim,[‖] Haley Vapnik, Stephen Cotty, Megan Aubin, Sonja Berensmeier, Akihiro Kushima, and Xiao Su*

Cite This: *ACS Appl. Mater. Interfaces* 2020, 12, 49713–49722

Read Online

ACCESS | Metrics & More | Article Recommendations | Supporting Information

ABSTRACT: Nanostructured polymer interfaces can play a key role in addressing urgent challenges in water purification and advanced separations. Conventional technologies for mercury remediation often necessitate large energetic inputs, produce significant secondary waste, or when electrochemical, lead to strong irreversibility. Here, we propose the reversible, electrochemical capture and release of mercury, by modulating interfacial mercury deposition through a sulfur-containing, semiconducting redox polymer. Electrodeposition/stripping of mercury was carried out with a nanostructured poly(3-hexylthiophene-2,5-diyl)-carbon nanotube composite electrode, coated on titanium (P3HT-CNT/Ti). During electrochemical release, mercury was reversibly stripped in a non-acid electrolyte with 12-fold higher release kinetics compared to nonfunctionalized electrodes. *In situ* optical microscopy confirmed the rapid, reversible nature of the electrodeposition/stripping process with P3HT-CNT/Ti, indicating the key role of redox processes in mediating the mercury phase transition. The polymer-functionalized system exhibited high mercury removal efficiencies (>97%) in real wastewater matrices while bringing the final mercury concentrations down to <2 μg L^{-1}. Moreover, an energy consumption analysis highlighted a 3-fold increase in efficiency with P3HT-CNT/Ti compared to titanium. Our study demonstrates the effectiveness of semiconducting redox polymers for reversible mercury deposition and points to future applications in mediating electrochemical stripping for various environmental applications.

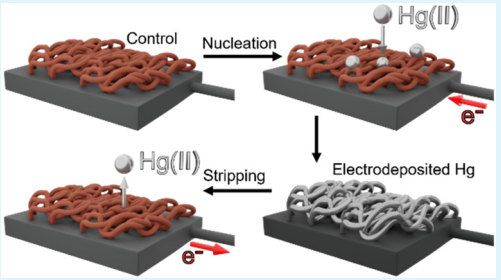

KEYWORDS: *semiconducting polymers, mercury remediation, electrochemical separations, electrodeposition, P3HT, functionalized interfaces, molecular selectivity*

INTRODUCTION

Mercury (Hg) is a widespread aqueous pollutant with pernicious effects, targeting primarily the nervous system, kidneys, and developing fetuses.[1] Mercury can occur in elemental (Hg(0)), inorganic (*e.g.*, mercuric (Hg(II)) and mercurous (Hg(I)) salts) and organic forms (*e.g.*, methylmercury).[2] In both marine and terrestrial environments, Hg is commonly found as Hg(II) complexes, often associated with inorganic or organic ligands.[3] In addition, atmospheric Hg enters watersheds and lake surfaces chiefly as divalent mercury.[2] Point source pollution of mercury can originate from various industrial sources such as a chlor-alkali process, poly(vinyl chloride) production, and pharmaceutical manufacturing, with waste streams featuring a broad Hg concentration range (10 μg L^{-1} to 10 mg L^{-1}).[4] Due to the adverse impacts of Hg, the U.S. Environmental Protection Agency (EPA) has set the maximum contaminant level of Hg in potable water to 2 μg L^{-1}, while the World Health Organization (WHO) established a maximum allowable level of 6 μg L^{-1}.[5,6]

Adsorbent materials play a critical role in water purification technologies,[7−9] including specific materials developed for the remediation of Hg from water.[10−17] However, traditional adsorption processes often require large quantities of chemical regenerants and additional post-treatment methods for reuse.[18] Furthermore, few of these materials are efficient in addressing the broad concentration ranges of mercury and the presence of competing species.[18] Finally, many mercury-selective adsorbents require the use of expensive raw materials or necessitate sophisticated preparation procedures.[19]

Electrochemically assisted processes can be a promising approach for mercury remediation, providing modularity and scalability, by controlling the capture and release of target ions through applied potential.[20−25] Tailoring the electrode surface with functional materials offers high selectivity and regenerability.[21−23,26−30] Polymeric systems can be attractive platforms for the electrochemically mediated capture and release

Received: August 29, 2020
Accepted: October 6, 2020
Published: October 20, 2020

https://dx.doi.org/10.1021/acsami.0c15570
ACS Appl. Mater. Interfaces 2020, 12, 49713–49722

of Hg, such as the use of polyaniline (PANI) for Hg(II) removal from water.[31] Electrochemical remediation of Hg(II) ions was also achieved *via* cathodic alloy formation using platinum electrodes, but the regeneration process required the use of strong acid (1 M HNO_3).[32] However, in general, electrochemically mediated Hg remediation has received limited attention in comparison with other heavy-metal contaminants,[21] and few studies exploring methods beyond electrosorption-based approaches.

Here, we investigate mercury remediation mediated by electrodeposition and stripping at an electroactive polymer interface. A semiconducting polymer, poly(3-hexylthiophene-2,5-diyl) (P3HT), was used as a functional interface to promote reversible electrodeposition and stripping (Figure 1).

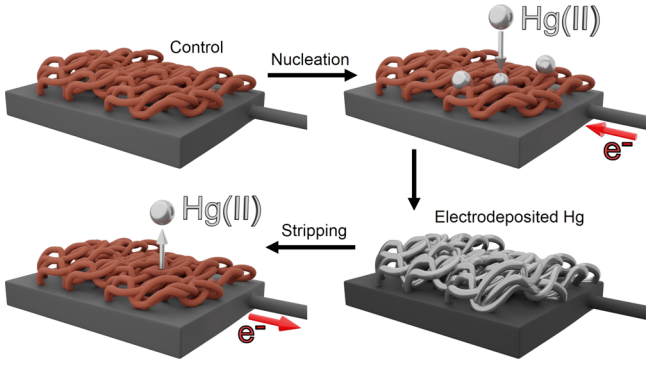

Figure 1. Schematic representation of the reversible capture and release of mercury. First, Hg(II) is captured (electrodeposited) on the P3HT-CNT/Ti electrode; during the subsequent step, Hg(0) is released (stripped) by applying an oxidizing potential.

While there have been extensive studies with pendant-group redox polymers for ion capture,[25−29] these main-chain semiconducting polymers have received limited attention in electrochemical separations, despite their interesting electroactive properties. P3HT has important applications in the field of organic photovoltaic devices and lithium-ion batteries as well as in oxidative photocatalysis.[33−37] P3HT can be oxidatively doped *via* potential control, introducing polarons and bipolarons (referred as $P3HT^+$).[38] Oxidizing P3HT increases the hole density and modifies the energetic distribution of charge carriers across the polymer, thus increasing P3HT conductivity and even promoting catalytic activity for oxidation reactions.[34,39,40]

By taking advantage of excellent processability and synergistic electrocatalytic properties of P3HT,[41] we developed an electrochemically mediated Hg removal technique with desirable features of rapid and reversible capture/release kinetics as well as cyclability of the electrodes. Our study performs a comprehensive analysis of the selectivity toward mercury, in the presence of competing species and real water matrices. In addition, we tracked in real-time the electrodeposition and stripping of Hg through *in situ* optical microscopy (*in situ* OM), showcasing the fast kinetics of a cycle of deposition/stripping enabled *via* the use of polymer-functionalized interfaces. Finally, an energy analysis for P3HT-mediated Hg removal was carried out, revealing significant improvement in energy efficiency compared to nonfunctionalized (bare metal) surfaces. Our findings demonstrate that semiconducting redox polymers enable reversible, rapid, and energy-efficient mercury remediation without the need for any external chemical regenerants. More broadly, our work provides important insights into the role of semiconducting electroactive interfaces for mediating electrodeposition and stripping.

RESULTS AND DISCUSSION

Hg Removal *via* Electrodeposition. We selected titanium (Ti) as a support, as it is more abundant and accessible than other noble-metal substrates, such as platinum,[32] and screening results showed significant Hg removal performance by rapid electrodeposition (Figure S1). P3HT-CNT/Ti electrodes were prepared by dip-coating in a suspension of P3HT and multiwalled carbon nanotubes using a titanium mesh as a substrate based on previous methodology for preparing metallopolymer electrodes.[42] The porosity of the interface was greatly enhanced by carbon nanotubes (CNT): when comparing BET surface area values of P3HT and P3HT-CNT, adding CNT determined a 7-fold increase of the electrode surface area, reaching 85.68 $m^2\ g^{-1}$ (Table S1). Furthermore, P3HT is highly soluble in many organic solvents[43,44] and has previously shown strong mixing with CNT owing to strong $\pi-\pi$ conjugated interactions,[45] resulting in a nanoporous structure with high ion accessibility and conductivity.

The standard reduction potential of mercury occurs within the electrochemical stability window of water ($Hg_2^{2+}{}_{(aq)} + 2e^- = 2Hg_{(liq)}$, $E^0 = +0.599$ V *versus* Ag/AgCl and $Hg^{2+}{}_{(aq)} + 2e^- = Hg_{(liq)}$, $E^0 = +0.657$ V *versus* Ag/AgCl),[46] enabling the electrodeposition of Hg(II) from contaminated aqueous solutions into metallic Hg on the surface of the electrode (Figure 1). First, we investigated the effect of the applied potential on the mercury removal efficiency with a 20 mM KNO_3 background electrolyte and observed a correlation between applied potential and the removal of mercury (Figure 2a). On P3HT-CNT/Ti electrodes at +0.25 V *versus* Ag/AgCl, <20% removal efficiency was obtained with initial Hg(II) concentrations of 1 and 10 mg L^{-1}, but >60% removal was observed with 200 mg L^{-1} Hg(II). Potentials lower than 0 V resulted in >75% removal efficiency in the case of 1 mg L^{-1} Hg(II) and >95% for 200 mg L^{-1} Hg(II) after 1 h. We attribute the main mechanism of mercury removal to electroplating, considering the high-reduction potential range of Hg. Upon prolonged charging of P3HT-CNT/Ti at −1.0 V (Figure 2b), the amount of electrodeposited mercury increased steadily with time. Figure 2b shows fast electroplating kinetics, reaching >800 $\mu g\ cm^{-2}$ after 180 min at −1 V. When comparing the kinetics of our deposition on P3HT-CNT/Ti with the previously reported Hg removal *via* alloy formation under similar operation conditions,[32] our system requires 1 h for the electrodeposition of 19.5 $\mu g\ cm^{-2}$ at 0 V as compared to ca. 4 h for alloy formation (see the Supporting Information for calculation details).

On the other hand, there was no discernible decrease in the concentration of Hg(II) when P3HT-CNT/Ti was left in contact with Hg(II) solution for 1−3 h without electrochemical potential (*i.e.*, at an open circuit, o.c.), again confirming that the removal was primarily electrochemically driven (Figure 2a,b). Even so, when the duration of the contact at the open circuit was largely extended to 3 days, a removal efficiency of 26% (corresponding to 18.4 mg Hg g^{-1} P3HT) was observed. In addition, a ultraviolet−visible spectrum of liquid-phase P3HT/chloroform solution exhibited a red-shift with a color change (from light brown to light purple) with the

https://dx.doi.org/10.1021/acsami.0c15570
ACS Appl. Mater. Interfaces 2020, 12, 49713−49722

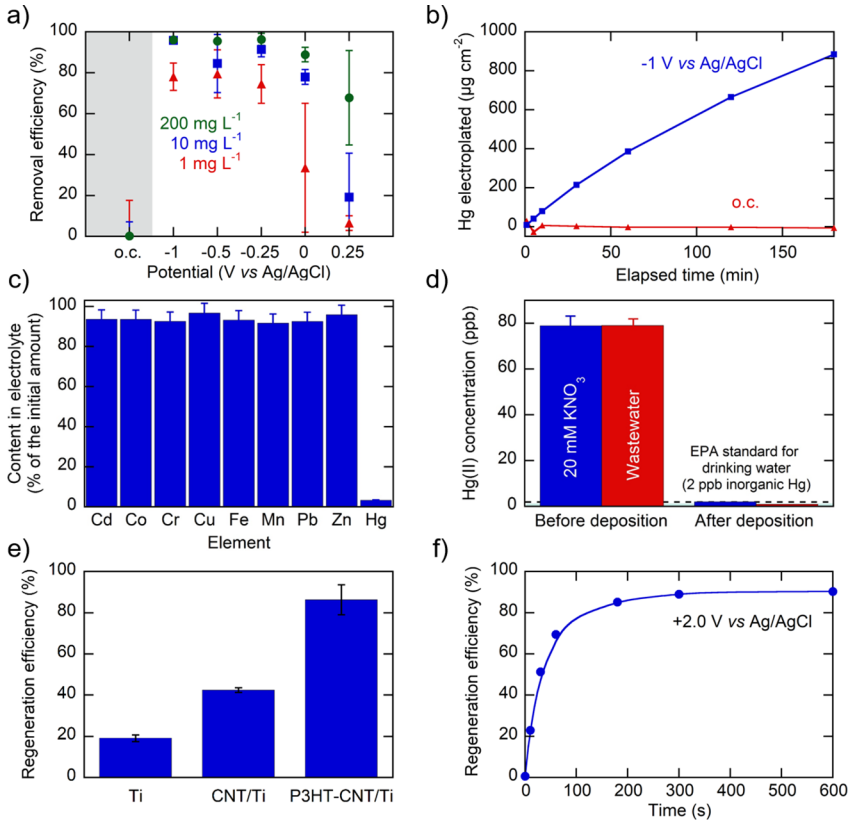

Figure 2. (a) Effect of applied potential and Hg(II) concentration on removal performance using a P3HT-CNT/Ti electrode (duration: 1 h). (b) Electrodeposition kinetics (initial Hg(II) concentration: 1 mM). (c) Element selectivity during electroplating using a P3HT-CNT/Ti electrode at 0 V *vs* Ag/AgCl for 1 h, in the presence of multiple competing metals, each at a starting concentration of 1 mM. (d) Removal of Hg(II) in 20 mM KNO_3 and municipal secondary wastewater effluent solution (from Urbana-Champaign Sanitary District). −1.0 V *vs* Ag/AgCl was applied for 5 h. (e) Regeneration efficiency for different electrode coatings. Electrodeposition for 0.5 h in 1 mM Hg(II) + 20 mM KNO_3 at −1.0 V, followed by +1.5 V for 0.5 h for releasing (stripping) deposited mercury into the 20 mM KNO_3 electrolyte. (f) Release kinetics at +2.0 V *vs* Ag/AgCl for P3HT-CNT/Ti.

addition of Hg(II) (Figure S2), implying the possibility of a soft−soft interaction between Hg(II) and sulfur, as also reported in previous studies.[47,48] It is hypothesized that the Hg(II) ions bound to thiophene are expected to be preferentially deposited in the metallic form on the polymer matrix, providing favorable active sites for subsequent deposition. A detailed mechanistic study is planned in the future to elucidate and confirm the exact mechanisms for the physical binding and subsequent electroplating of Hg(II) on P3HT interfaces.

Selectivity of Separation Over Competing Species. Selectivity over common interfering substances, such as heavy metals and organic compounds, is an important factor for practical applications. P3HT-CNT was first tested in a 20 mM KNO_3 matrix spiked with 1 mM of cadmium, cobalt, chromium, copper, iron, manganese, lead, zinc, and mercury. After a chronoamperometry at −0.25 V for 1 h, the final concentration of mercury decreased to about 1.1% of its initial concentration, showing that the efficiency for mercury removal was not affected by the presence of other metals (Figure S4). While the concentrations of most metals did not decrease significantly, copper decreased by 98.4% due to its relatively positive reduction potential that leads to co-deposition with mercury.[49] The remarkable selectivity in capturing mercury was enabled by setting the applied potential to 0 V *versus* Ag/AgCl, a potential level where only mercury electrodeposition is thermodynamically feasible while the other metals, including copper, cannot be electroplated. As shown in Figure 2c, only mercury exhibited a significant decrease in concentration featuring a removal efficiency greater than 96%. This result confirmed that the positive-reduction potential of mercury enables selective remediation by controlling applied potential in the electrodeposition process. Furthermore, the removal of mercury was not affected by the presence of humic acid, a common organic competing species (Figure S5). To explore the removal efficiency of Hg in a real wastewater matrix at environmental concentrations, we investigated the performance of P3HT-CNT/Ti using 20 mM KNO_3 and real secondary effluent wastewater (collected from Urbana-Champaign Sanitary District), spiked with 78−79 $\mu g\ L^{-1}$ Hg(II). Over 97.5% removal efficiency was achieved after a 5 h deposition at −1.0 V for both water matrices (Figure 2d), satisfying the 2 $\mu g\ L^{-1}$ EPA standard. These results demonstrate that the electrical modulation of P3HT-functionalized electrodes enables efficient Hg remediation for real-world, practical applications.

Reversible Nature of Hg Deposition and Release on P3HT-CNT/Ti. Here, the benefit of implementing P3HT-CNT/Ti as an electrode material was investigated by first charging the P3HT-CNT/Ti electrode in 200 mg L^{-1} (1 mM) Hg(II) + 20 mM KNO_3 at −1.0 V during electrodeposition for 0.5 h and then by applying +1.5 V for 0.5 h for releasing (stripping) deposited mercury into a 20 mM KNO_3 electrolyte. As depicted in Figure 2e, P3HT-CNT/Ti exhibited the highest

https://dx.doi.org/10.1021/acsami.0c15570
ACS Appl. Mater. Interfaces 2020, 12, 49713−49722

regeneration efficiency (defined as the ratio of mercury recovered to deposited), at 86.3% of regeneration without the use of acid or any other chemical additive. Release kinetics revealed that regeneration was completed within 10 min upon charging with positive potential (Figure 2f), demonstrating the rapid kinetics of stripping. The release rate is orders-of-magnitude superior to release from amalgamated platinum and also from PANI (see the Supporting Information for calculation details).[31,32] On the other hand, nonfunctionalized CNT/Ti or Ti showed poorer regeneration (Figure 2e), implying irreversible and/or the slow nature of anodic stripping. Hg stripping in strong acid (1.1 M HNO_3) showed the same trend in the regeneration efficiency (Figure S3). This result confirmed that the judicious selection of materials enabled not only efficient removal *via* electrodeposition but also electrochemically controlled release for cyclability.

The reversible nature of deposition and release of mercury on P3HT-CNT/Ti can also be confirmed through scanning electron microscopy (SEM) and energy-dispersive spectroscopy (EDS) analyses. First, as shown in Figure 3a, pristine

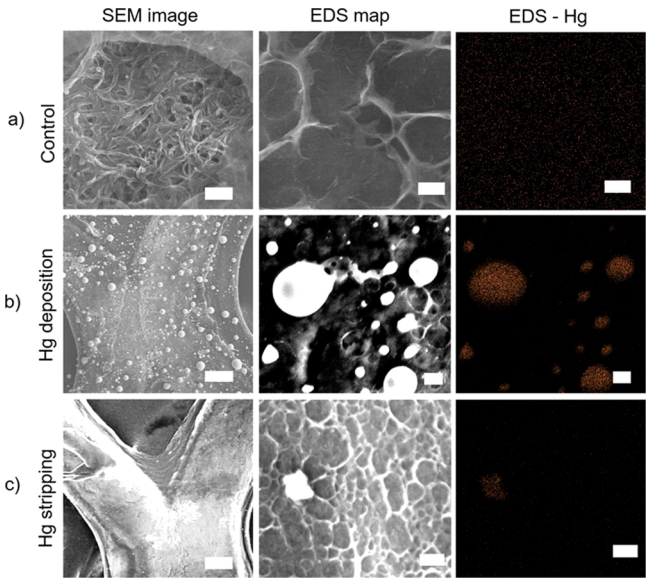

Figure 3. SEM-EDS images of P3HT-CNT/Ti electrodes: (a) pristine, (b) after Hg electrodeposition, and (c) after Hg stripping. In SEM images, scale bar is 200 nm (a) and 50 μm (b, c). EDS mapping confirms that the nuclei consist of Hg. In EDS images, the scale bar is 1 μm (a) and 2 μm (b, c).

P3HT-CNT/Ti electrodes feature a homogenous and nanoporous morphology. The high-resolution SEM image after electrodeposition (Figure 3b) shows the presence of metallic mercury deposited on P3HT-CNT/Ti coating upon the application of a reducing potential, and EDS mapping confirmed that indeed the agglomerate formed on the P3HT-CNT/Ti surface consists of Hg. SEM imaging of bare titanium electrodes after electrodeposition also displayed metallic Hg with similar features to P3HT-CNT/Ti electrodes (Figure S12a,b). Here, it must be emphasized that drying the mercury-coated electrode in air drastically changes the morphology and size of deposited Hg, *i.e.*, small Hg particles coalesce into bigger droplets very rapidly after that the surrounding water layer is dried. This change in Hg surface distribution upon drying has also been reported by Wu *et al.* for glassy carbon electrodes substrates with Hg(II) in the 20–200 mg L^{-1} range.[50] As expected, SEM-EDS analysis (Figure 3b) showed the formation of large, spherical mercury droplets, thereby underscoring the challenge of precisely analyzing surfaces containing electrodeposited mercury with *ex situ* type methods. As will be discussed later, *in situ* optical microscopy offers a direct observation tool for the surface phenomena occurring on P3HT-CNT/Ti electrodes during deposition and stripping. After applying a positive potential for stripping, the regeneration of P3HT-CNT/Ti electrodes was evident through SEM-EDS analysis (Figure 3c), contrary to Ti, which showed incomplete regeneration (Figure S12c,d), further proving the reversible nature of P3HT-CNT/Ti electrodes for electrochemically controlled capture and release of mercury.

Cyclic voltammetry (CV) characterization was carried out to further investigate the reversibility of P3HT-CNT/Ti for the capture and release of mercury compared to Ti as a control. First, we observed that the background current for the Ti substrate in the −1.0 to +1.5 V potential range was low ($|i| < 0.05$ mA cm^{-2}) without the addition of Hg(II) in 20 mM KNO_3 (Figure S6a), and no cathodic reaction, including hydrogen evolution, occurred in the cathodic scan up to −1.0 V. On the other hand, the presence of 200 mg L^{-1} (1 mM) Hg(II) brought about a cathodic current from <+0.20 V, which is attributed to the electrodeposition of Hg(II) from solution (Figure S6a). Electrochemical deposition of metal ions on a foreign surface requires higher overpotential compared to deposition on the same metal because of the crystallographic substrate−metal misfit.[51] Therefore, deposition of Hg on foreign surfaces (*e.g.*, Ti in this study) necessitated a more negative potential for the onset of electrodeposition ($E_{nucleation}$) compared to the redox potential of Hg(II)/Hg(0) (E_{eq}). On the other hand, in the anodic scan, the oxidation of Hg(0) to Hg(II) started from a surface already coated with Hg, resulting in an onset potential of stripping close to the equilibrium potential of Hg(II)/Hg(0) (E_{eq}). The difference between $E_{nucleation}$ and E_{eq} represents the nucleation overpotential ($\eta_{nucleation} = |E_{nucleation} - E_{eq}|$), and the current−potential curves in the cyclic voltammetry exhibit a crossover between the cathodic and anodic scans, which is indicative of the formation of Hg nuclei on the electrode.[51] In Figure S6a, during the cathodic scan, no significant increase in current occurred up to ca. +0.2 V; this potential threshold can be interpreted as the onset for nucleation, $E_{nucleation}$. On the anodic scan, deposition proceeded on the existing Hg surface until E_{eq} was reached (0.46 V, the *x*-intercept in the CV plot). After passing E_{eq}, a peak corresponding to the oxidation of deposited Hg can be seen, which is associated with stripping. However, depending on the negative potential limit of CV, sometimes, no stripping peak was observed (Figure S6b), indicating the irreversible nature of mercury electrodeposition/stripping on Ti. The irreversibility of Ti electrodes was probably associated with the native oxide layer on the surface of the substrate: this semiconducting layer was responsible for high resistance against anodic stripping, which is larger than the resistance against cathodic deposition, as reported previously.[52]

In the case of P3HT-CNT/Ti (Figure 4a), the background current in the absence of Hg(II) exhibited the characteristic oxidation behavior of P3HT to $P3HT^+$, with an onset potential of 0.62 V, coupled with anion doping (Figure 4b). In the presence of Hg(II) ions, P3HT-CNT/Ti displayed a cathodic current with the onset at a potential of +0.30 V for mercury electrodeposition (Figure 4a), which is indicative of lower

https://dx.doi.org/10.1021/acsami.0c15570
ACS Appl. Mater. Interfaces 2020, 12, 49713−49722

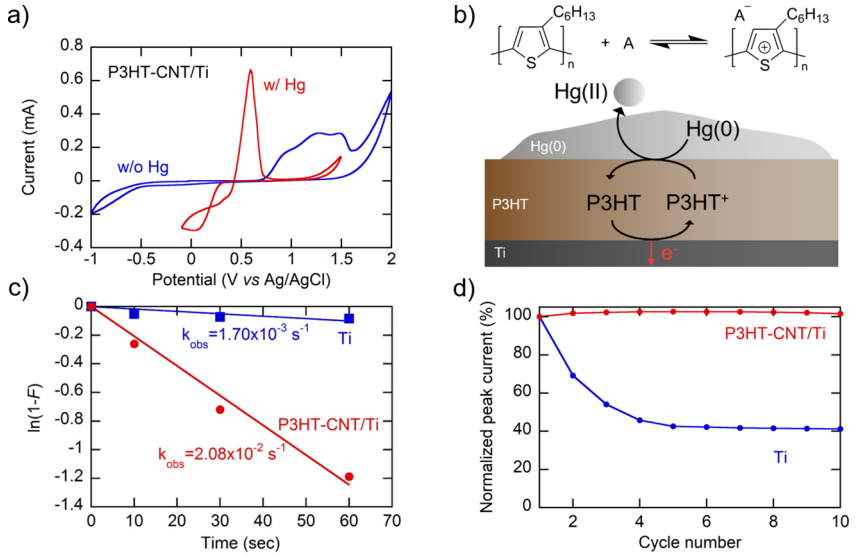

Figure 4. (a) Cyclic voltammetry of P3HT-CNT/Ti electrodes in the 20 mM KNO_3 electrolyte in the absence (blue) and presence of 1 mM Hg(II) (red) with a 50 mV s^{-1} scan rate. (b) The oxidative doping of P3HT upon positive charging and a schematic representation of Hg stripping mediated by the redox reaction of $P3HT^+$/P3HT. (c) Hg stripping kinetics at 2.0 V *vs* Ag/AgCl. Before stripping, Hg was electrodeposited at −1.0 V in 20 mM KNO_3 + 1 mM Hg(II) for 10 min. (d) Normalized peak anodic current over 10 cycles. Complete CV is shown in Figure S7.

nucleation overpotential ($\eta_{nucleation}$) compared to Ti electrodes (Figure S6c). Given that the nucleation of Hg(II) preferentially starts on step edges and on surface defects and that the P3HT-CNT/Ti surface is more defect-rich,[53,54] we hypothesized that the P3HT-CNT surface might facilitate Hg nucleation as compared to bare Ti, exhibiting a lower overpotential for the onset of the cathodic current. The current at −1.0 V was smaller with the P3HT-CNT/Ti electrode as compared to Ti (Figure S6b) due to lower electrical conductivity of the P3HT-CNT/Ti composite compared to Ti metals.[35,55] This was in agreement with mercury removal performance at −1.0 V with Ti and P3HT-CNT/Ti; the removal efficiency at −1.0 V was higher with Ti compared to P3HT (Figure S1). Nevertheless, although capturing a smaller amount of metallic mercury on its surface, P3HT-CNT/Ti showed a significantly larger anodic peak (Figures S6b and S7), which could be interpreted as the reversible, facilitated oxidation of the electroplated mercury. All these electrochemical characterizations are in agreement with the regeneration efficiency (Figure 2e) and SEM-EDS analysis (Figure 3) and demonstrate that P3HT-CNT/Ti enables reversible oxidation of metallic mercury, as compared to bare Ti, which is only able to plate mercury but not to release it effectively.

We attribute the high regeneration efficiency to the coupled effect of the increased P3HT conductivity upon oxidation and the associated electrocatalytic properties of the polymer. P3HT is nonconducting in the neutral state but becomes conductive when oxidized because of the delocalization of electrons along the polymer backbone (Figure 4b),[36] thereby facilitating electron transfer and the phase transition.[52] XPS analysis confirmed that for higher applied potentials, *i.e.*, during stripping, the percentage of oxidized P3HT increased; this behavior was observed both in non-acid and acid electrolytes (Figure S9). Furthermore, our CV analysis revealed that the onset potential of P3HT oxidation is 0.62 V (Figure 4a), implying that oxidized P3HT ($P3HT^+$) is electrophilic and a strong electron acceptor, while for metallic Hg, whose oxidation onset potential is 0.44 V on P3HT-CNT/Ti surface, it was relatively easier to donate electrons to $P3HT^+$. Hence, thermodynamically favorable, mediated electron transfer from Hg(0) to $P3HT^+$, followed by the regeneration of $P3HT^+$ *via* direct anodic reaction, is thought to facilitate the stripping process of Hg(0) in the P3HT-CNT/Ti system (Figure 4b). In fact, a 12-fold increase in initial stripping kinetics was recorded, with k_{obs} (observed rate constant) being 2.08×10^{-2} s^{-1} for P3HT-CNT/Ti, compared to 1.70×10^{-3} s^{-1} for Ti (Figure 4c). In this process, CNT is thought to facilitate the redox-mediated charge transfer by providing a large active surface area with high conductivity, as reflected by the greatly improved regeneration efficiency achieved with the incorporation of CNT (Figure S3b). Even more, the coulombic efficiency of stripping with P3HT-CNT/Ti was 37.4%, 4 times higher than that of Ti (9.6%, Figure S14); the remainder of the electrons flowing is thought to be devoted to the redox reactions of P3HT, which was not connected to Hg(0) oxidation.

In addition, P3HT-CNT/Ti not only improved the reversibility but also exhibited higher performance stability upon oxidation and reduction over a number of cycles. As shown in Figure 4d, peak current density for 10 cycles (normalized by the peak current at the first cycle) showed a stable, reversible mercury capture and release enabled by P3HT (the complete CVs are reported in Figure S7). Continuous charging−discharging of P3HT-CNT/Ti for 50 cycles did not diminish mercury removal performance, indicating reversible, stable nature of the semiconducting interfaces (Figure S8). On the other hand, not only did Ti have very small electrochemical activity for the stripping of deposited Hg but it also featured decreasing peak current over 10 cycles (Figure 4d, the complete CVs are reported in Figure S7). Significant irreversibility can be seen from a drop of 40% of the anodic peak current. All these results further reaffirm the key role of P3HT-coated interfaces in providing high electrocatalytic activity, reversibility, and stability.

***In situ* Optical Microscopy.** We employed *in situ* optical microscopy (*in situ* OM) to precisely observe mercury electrodeposition/stripping at our polymer films, allowing the

https://dx.doi.org/10.1021/acsami.0c15570
ACS Appl. Mater. Interfaces 2020, 12, 49713−49722

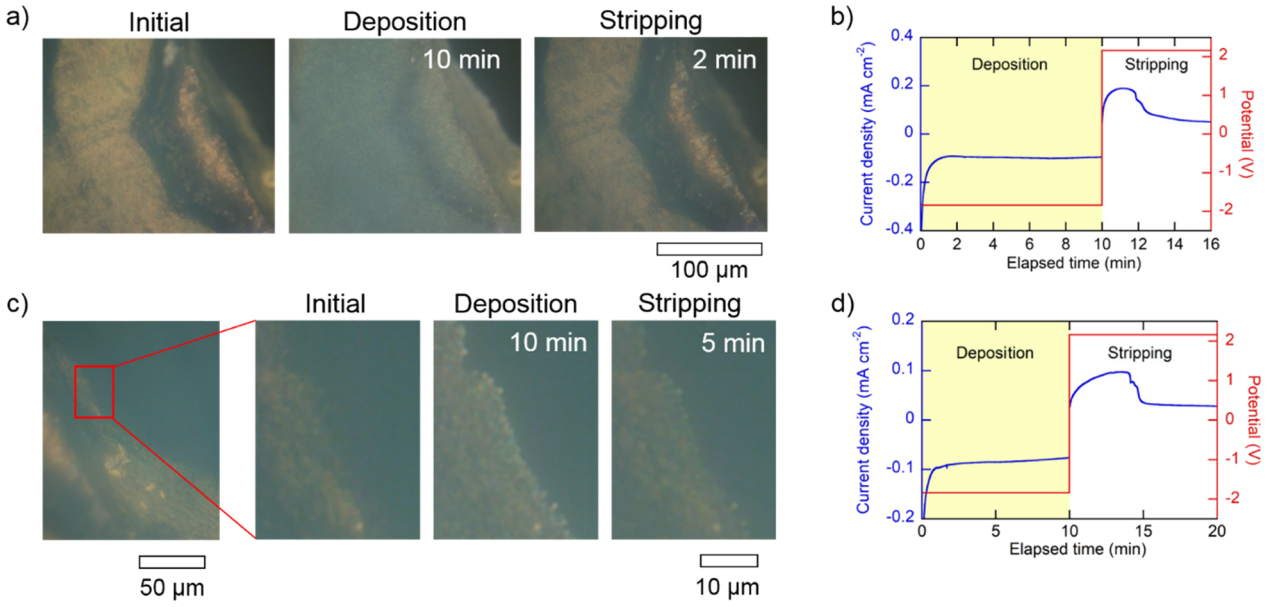

Figure 5. *In situ* optical microscopy of Hg electrodeposition and stripping on P3HT-CNT/Ti electrodes, in two-electrode configuration. (a, b) Low magnification overview with the corresponding current−time behavior during electrodeposition/stripping. (c, d) Detail of the electrode edge and corresponding current−time behavior. A clear oxidation peak can be observed during stripping, associated with the release of Hg from the interface during the same time span. Electrodeposition at −2.0 V, followed by stripping at +2.0 V.

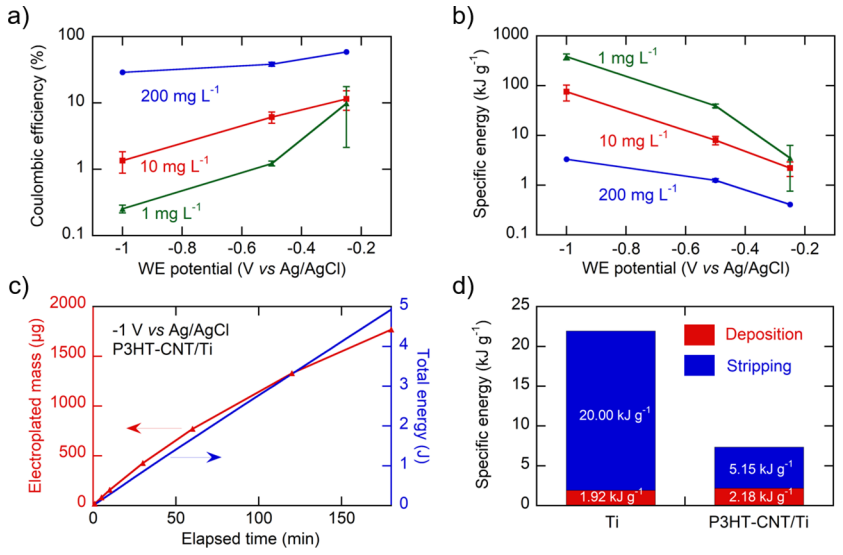

Figure 6. (a) Coulombic efficiency and (b) specific energy as a function of the working electrode (WE) potential during Hg(II) electrodeposition on P3HT-CNT/Ti. (c) Electrodeposition kinetics and total energy consumption during electroplating on P3HT-CNT/Ti. (d) Comparison of the specific energy for electrodeposition/stripping: deposition at −1.0 V *vs* Ag/AgCl with 1 mM Hg(II) and stripping at +2.0 V in 20 mM KNO_3.

direct tracking of changes in interface morphology in real-time during electrochemical treatment, as demonstrated for other systems.[56,57] Applying a cell voltage of −2 V (two-electrodes electrochemical cell) revealed the formation of a uniform film on P3HT-CNT/Ti-coated electrodes, as displayed in Figure 5a,c, which was attributed to the deposition of mercury. Contrary to indirect *ex situ* techniques (*e.g.*, SEM in Figure 3), *in situ* OM did not interfere with the deposition morphology of Hg, thus allowing for the observation of the surface mechanisms during the cycle of deposition and stripping. In particular, we observed that the deposited Hg film was released rapidly (<10 min) in the same Hg-containing solution by reversing polarity and applying 2 V so that the regenerated P3HT-CNT/Ti surface was promptly recovered (Figure 5a,c); this is in agreement with the fast stripping kinetics of P3HT-CNT/Ti (Figures 2f and 4c), which is attributed to the enhanced electrochemical activity by redox-mediated oxidation of Hg(0).*In situ* OM not only allows to track morphological changes in real time but also enables us to couple the observed surface transformations with the electrochemical response of the material, by simultaneously comparing the current−time features with the OM imaging. For instance, a current peak in the chronoamperometry curve was observed, which can be associated to the rapid surface regeneration highlighted by *in situ* OM during the same time interval of the peak duration (Figure 5a−d). Hence, this coupled imaging/electrochemical characterization clearly showed the rapid Hg capture/release process, triggered by potential control. By focusing on the edge

https://dx.doi.org/10.1021/acsami.0c15570
ACS Appl. Mater. Interfaces 2020, 12, 49713−49722

of the polymer, we confirmed that the film consists indeed of small mercury particles, which were completely dissolved during stripping and are shown in Figure 5c,d. This provides direct evidence of the fast plating and stripping performance when using P3HT-CNT/Ti by which reversible behavior is achieved in a non-acid medium, thus removing the need for additional chemical regenerants in a practical application.

In comparison, Ti electrodes displayed an incomplete stripping of the electroplated Hg. During electrodeposition, Hg particles formed on the electrode surface, and by carefully tracking them during the subsequent stripping step using the optical microscope, it was evident that only few of these Hg particles disappeared (green arrows, Figure S10a). Additionally, the current−time curve (Figure S10b) did not feature a marked oxidation peak during stripping, contrary to P3HT-CNT/Ti (Figure 5b,d). Furthermore, SEM results confirmed that the release of Hg with Ti electrodes occurred to a much lesser extent as compared to P3HT-CNT/Ti (Figure S12c,d). All these characterizations converge to the conclusion that Ti electrodes perform poorly during Hg release. Notably, *in situ* OM results provided insights into how Hg distribution and deposition morphology changes as the electrode is dried; Figure S11 shows that drying the P3HT-CNT/Ti electrode in the air causes the coalescence of the deposited Hg into droplets of bigger sizes within a short time period (~63 s). The observed change in Hg distribution upon drying underscores the need of *in situ* imaging techniques for a correct Hg deposition morphology characterization.

Energy Consumption Analysis. Finally, we estimated the energy consumption for the working electrode half-cell reaction during electrodeposition and stripping, as reported in Figure 6. The following equation was used

$$SE = \frac{\int_0^t E(t) i(t)\, dt}{m_{Hg}} \quad (1)$$

Eq 1 estimates the specific energy (SE in kJ g^{-1}) during electrodeposition (or stripping) by integrating the product of the working electrode potential $E(t)$ by the current $i(t)$ over the duration of the electrochemical deposition (or stripping) and dividing it by the deposited (or stripped) Hg mass m_{Hg}; the specific energy represents the energy consumed by the working electrode half-cell during electrodeposition or stripping. For electrodeposition, Hg(II) concentration and applied potential affect both the coulombic efficiency (Figure 6a) and the specific energy (Figure 6b); higher overpotentials (*e.g.*, at −1 V) resulted in lower coulombic efficiency and more energy consumption for electrodeposition. At higher Hg(II) concentrations, coulombic efficiency was improved and specific energy was lowered, as displayed in Figure S15 for P3HT-CNT/Ti in the case of −1 V. In the case of a 3 h prolonged electrodeposition on P3HT-CNT/Ti in 200 mg L^{-1} Hg(II) at −1 V, we estimated the specific energy (as the ratio of the total energy to the electroplated mass) as a function of time (Figure 6c). The specific energy of P3HT-coated electrodes slightly increased over time (1.6−2.8 kJ g^{-1} range), indicating the importance to control the duration in practice (Figure S13). Ti is slightly more efficient for electrodeposition as compared to P3HT-CNT/Ti (Figure 6d); this is in accordance with the less conductive nature of neutral P3HT-CNT/Ti during deposition, as discussed previously (Figure S1). Nevertheless, P3HT-CNT/Ti is much more efficient than Ti during stripping at 2 V (Figure 6d), especially due to improved kinetics (Figure 4c) and coulombic efficiency (Figure S14). As a result, P3HT-CNT/Ti electrodes exhibit a 3-fold improvement in total energy efficiency compared to Ti (Figure 6d, 7.33 kJ g^{-1} for P3HT-CNT/Ti *vs* 21.92 kJ g^{-1} for Ti), further confirming that judicious selection of materials enables the energy-efficient removal of Hg. These results demonstrate that P3HT-CNT/Ti not only allows reversible uptake and release of Hg but also provides an energy-efficient option for electrochemical Hg remediation.

CONCLUSIONS

In summary, we propose an efficient mercury remediation technique based on the electrochemical reversible capture and release of Hg(II) in aqueous solution, modulated by an electroactive polymer. We explored the interfacial control of electrodeposition and stripping through the redox semiconducting polymer P3HT, which facilitates the stripping of deposited mercury. First, Hg(II) was removed *via* electrodeposition on P3HT-CNT/Ti electrodes with potential control, and the performance of P3HT-CNT/Ti was further benchmarked using real wastewater samples spiked with ultra-diluted Hg. During the regeneration of P3HT-CNT/Ti, deposited Hg was stripped in a non-acid medium with high regeneration efficiency and 12-fold faster release kinetics enabled with P3HT-CNT/Ti compared to Ti, the unfunctionalized Ti surface only allowing for deposition but not release. Cyclic voltammetry analysis highlighted the nucleation behavior of Hg and the enhanced electrochemical response during the anodic scan, demonstrating the synergistic interplay of the redox-mediated catalysis and enhanced conductivity of $P3HT^+$. We further monitored the reversible capture/release in real time using *in situ* optical microscopy, confirming uniform Hg deposition and rapid release. An analysis of energy consumption for Hg(II) capture revealed that P3HT-CNT/Ti electrodes enhance energy efficiency by 3-fold, compared to bare titanium, with the majority of the energy savings coming from the more efficient stripping process when using a semiconducting polymer.

Our studies demonstrate an efficient system for the electrochemically controlled capture and release of Hg, without requiring chemical regenerants or causing secondary pollution, which could be deployed for on-site remediation of mercury in aqueous waste streams. Our proof-of-concept illustrates the remarkable capabilities of semiconducting polymer interfaces to enable reversible and energy-efficient Hg electrodeposition and stripping, which expands the existing redox-material library for electrochemical separations. We expect our studies to provide general insights into electrodeposition and stripping at rationally designed functional interfaces and pave a method for semiconducting polymers to be used in water purification applications.

EXPERIMENTAL SECTION

Preparation of P3HT-CNT/Ti Electrodes. Electrode preparation was adapted from previously reported procedures.[42] Solution A was made by mixing P3HT (16 mg) (regioregular electronic grade, Rieke Metals) with CNT (8 mg) (multiwalled carbon nanotubes, Sigma-Aldrich) in chloroform (2 mL) followed by sonication (30 min) in icy water. Solution B was prepared by mixing CNT (8 mg) in chloroform (2 mL) followed by sonication (30 min) in icy water. Solution B was then poured in solution A and further sonicated (30 min) in icy water; this solution is referred to as P3HT-CNT. Titanium-grade 1 mesh (titanium screen, Fuel Cell Store) rectangles (1 cm × 2 cm, 53 μm thick) were cut and coated with P3HT-CNT *via* dip coating. The

https://dx.doi.org/10.1021/acsami.0c15570
ACS Appl. Mater. Interfaces 2020, 12, 49713−49722

dipped area was 2 cm^2 (sum of the front and back side each having 1 cm × 1 cm surface area) and after each dip, the solvent was allowed to evaporate. CNT/Ti electrodes were prepared in the same way, using CNT dispersed in chloroform (4 mg mL^{-1}) and by sonicating (60 min) in icy water. The polymer-coated electrodes were secured to a copper wire using copper foil tape. Poly(vinyl)ferrocene (Polyscience)-carbon nanotube composite on Ti mesh (PVF-CNT/Ti) electrodes was prepared with the same steps as the P3HT-CNT/Ti electrodes, except with PVF being the polymer instead of P3HT.

Hg Capture and Release Experiments. Hg(II) solutions with concentrations of 1, 10, and 200 mg L^{-1} Hg(II) + 20 mM KNO_3 were prepared by mixing $Hg(NO_3)_2$ (puriss p.a., Sigma-Aldrich) and KNO_3 (Sigma-Aldrich) in DI water; these concentrations correspond to 0.005, 0.050, and 1 mM Hg(II), respectively. The potentiostats used were a VersaSTAT 4 potentiostat galvanostat (Princeton Applied Research) and a SP-200 (BioLogic). A 3-electrode electrochemical cell was used, with an Ag/AgCl (3 M NaCl) reference electrode (RE-5B Ag/AgCl, BASi) and a platinum wire counter electrode (CE). All electrodeposition and stripping experiments were done with a 20 mM KNO_3 background electrolyte, using 5 mL of solution in a 20 mL glass vial, and a 2 cm^2 electrode area, with magnetic stirring (300 rpm), unless otherwise stated. Electrodeposition kinetics was run with 15 mL of solution. Wastewater electrodeposition tests were carried out with 1 mL of solution, and a 2 cm^2 electrode area. When applying voltages >+0.2 V, a custom-made confinement for the CE (consisting of a pipette tip with a glass frit) minimized the plating of Hg on the CE. ICP-OES (5110 ICP-OES, Agilent Technologies) allowed to determine the Hg concentration in the solutions. The viewing mode was axial, 10 replicates were run, and the wavelengths 184.887, 194.164, and 253.652 nm were measured, using 194.164 nm for the removal and regeneration efficiency calculations. Rinse time was 90 s with a 1.1 M HNO_3 + 1 mg L^{-1} Au(III) rinse solution (prepared with $AuCl_3$), while all the dilutions were prepared with 1.1 M HNO_3 + 5 mg L^{-1} Au(III). This setup, adapted from Zhu *et al.*, allowed to overcome the memory effect of Hg.[58]

Hg stripping Kinetics. For the stripping experiments, electrodeposition was carried out at −1.0 V in 200 mg L^{-1} Hg(II) + 20 mM KNO_3 for 10 min (volume = 5 mL, electrode area = 2 cm^2, initial Hg mass present on the electrode = 311.7 μg). For the subsequent release, + 2.0 V was applied for 10 min. The observed reaction rate constant (k_{obs}) was estimated from the slope of the Hg(0) oxidation *vs* the time curve using the following equation

$$\ln(1 - F) = -k_{obs} \cdot t \quad (2)$$

where $F = C_t/C_o$, C_t is the amount of stripped Hg cation at time t, and C_o is the amount of deposited Hg.

Material Characterization. The surface morphologies and elemental mapping images of the electrodes were obtained using a scanning electron microscope (SEM; Hitachi S-4700 and JSM-7000F) operated at an accelerating voltage in the 10−20 kV range, equipped with energy-dispersive X-ray spectroscopy (EDS; iXRF) with the accelerating voltage in the 15−20 kV range and 30° take-off angle. EDS mapping of Hg reports the Mα emission energy of Hg. The surface areas of P3HT and P3HT-CNT were measured with Brunauer−Emmett−Teller analysis (BET, 3Flex Surface Characterization Analyzer, Micromeritics). The degree of oxidized P3HT was estimated using X-ray photoelectron spectroscopy (XPS; Kratos Axis ULTRA) with a monochromatic Al Kα X-ray source (210 W). The XPS results were analyzed using CASA XPS software (UIUC license). Binding energies were corrected to the alkyl C 1 s feature at 284.6 eV. S2p spectra were fitted with 100% Gaussian peaks with a linear baseline correction, following Ratcliff *et al.*[59] Hg could not be characterized using XPS due to equipment limitations for mercury at high-vacuum condition.

In situ Optical Microscopy Observation. Direct observation of the mercury deposition and stripping process was performed using a confined liquid cell. The cell was made using a glass slide, silicon elastomer films, and a cover glass (Figure S16). Ti and P3HT-CNT/Ti electrodes were cut to a small strip (4.0 mm × 2.0 mm) and used as the working electrode. An aluminum strip was used as the counter electrode. These electrode strips were sandwiched between the two elastomer films with a square window and placed on a glass slide. The cell was filled with a solution of Hg(II) in DI water (190 mg L^{-1}), and the top was closed with a cover glass for the optical microscope observation. The potentiostat used in these experiments was a Metrohm Autolab PGSTAT101.

■ ASSOCIATED CONTENT

Supporting Information

The Supporting Information is available free of charge at https://pubs.acs.org/doi/10.1021/acsami.0c15570.

Electrode material effect on removal efficiency, UV−vis spectra, electrode material effect on regeneration efficiency, competitive separation, effect of humic acid, cyclic voltammetry, stability of electrode, XPS, titanium electrode in situ optical microscopy, P3HT-CNT/Ti electrode drying tracked via in situ optical microscopy, titanium electrode SEM images, specific energy consumption, coulombic efficiency, and BET surface area (PDF)

P3HT-CNT/Ti*in situ* optical microscopy footage, low magnification overview (MOV)

P3H-CNT/Ti *in situ* optical microscopy footage, detail of the electrode edge (MOV)

Titanium electrode *in situ* optical microscopy footage (MOV)

P3HT-CNT/Ti electrode drying footage (MOV)

■ AUTHOR INFORMATION

Corresponding Author

Xiao Su − *Department of Chemical and Biomolecular Engineering, University of Illinois at Urbana-Champaign, Urbana, Illinois 61801, United States;* orcid.org/0000-0001-7794-290X; Email: x2su@illinois.edu

Authors

Riccardo Candeago − *Department of Chemical and Biomolecular Engineering, University of Illinois at Urbana-Champaign, Urbana, Illinois 61801, United States*

Kwiyong Kim − *Department of Chemical and Biomolecular Engineering, University of Illinois at Urbana-Champaign, Urbana, Illinois 61801, United States*

Haley Vapnik − *Department of Chemical and Biomolecular Engineering, University of Illinois at Urbana-Champaign, Urbana, Illinois 61801, United States*

Stephen Cotty − *Department of Chemical and Biomolecular Engineering, University of Illinois at Urbana-Champaign, Urbana, Illinois 61801, United States*

Megan Aubin − *Advanced Materials Processing and Analysis Center, Department of Materials Science and Engineering, University of Central Florida, Orlando, Florida 32816, United States*

Sonja Berensmeier − *Bioseparation Engineering Group, Department of Mechanical Engineering, Technical University of Munich, Garching 85748, Germany;* orcid.org/0000-0002-4943-848X

Akihiro Kushima − *Advanced Materials Processing and Analysis Center, Department of Materials Science and Engineering, University of Central Florida, Orlando, Florida 32816, United States;* orcid.org/0000-0001-5166-4198

Complete contact information is available at: https://pubs.acs.org/10.1021/acsami.0c15570

https://dx.doi.org/10.1021/acsami.0c15570
ACS Appl. Mater. Interfaces 2020, 12, 49713−49722

Author Contributions

[‖]R.C. and K.K. contributed equally.

Funding

The work was funded by startup funds from the University of Illinois Urbana-Champaign, and supported by an NSF CBET grant #1931941 to X.S. and a seed grant from the Illinois Water Resources Center Annual grant to X.S.

Notes

The authors declare no competing financial interest.

■ ACKNOWLEDGMENTS

SEM and XPS characterizations were carried out in the Frederick Seitz Materials Research Laboratory Central Research Facilities, University of Illinois. The authors thank P. B. Medina for assistance with experiments, and Dr. P. Fraga García and Prof. S. Dirè for valuable feedback.

■ REFERENCES

(1) Hassett-Sipple, B.; Swartout, J.; Schoeny, R.; Mahaffey, K. R.; Rice, G. E. *Mercury Study Report to Congress. Volume V: Health Effects of Mercury and Mercury Compounds*; U.S. Environmental Protection Agency: 1997; *V*.

(2) Darbha, G. K.; Ray, A.; Ray, P. C. Gold Nanoparticle-Based Miniaturized Nanomaterial Surface Energy Transfer Probe for Rapid and Ultrasensitive Detection of Mercury in Soil, Water, and Fish. *ACS Nano* **2007**, *1*, 208−214.

(3) Asaduzzaman, A.; Riccardi, D.; Afaneh, A. T.; Cooper, S. J.; Smith, J. C.; Wang, F.; Parks, J. M.; Schreckenbach, G. Environmental Mercury Chemistry - in Silico. *Acc. Chem. Res.* **2019**, *52*, 379−388.

(4) Cyr, P. J.; Suri, R. P. S.; Helmig, E. D. A Pilot Scale Evaluation of Removal of Mercury from Pharmaceutical Wastewater Using Granular Activated Carbon. *Water Res.* **2002**, *36*, 4725−4734.

(5) *2018 Edition of the Drinking Water Standards and Health Advisories Tables*. U.S. Environmental Protection Agency: Washington, DC, 2018.

(6) *Mercury in Drinking-Water: Background Document for Development of Who Guidelines for Drinking-Water Quality*; World Health Organization: Geneva, Switzerland, 2005.

(7) Nagar, A.; Pradeep, T. Clean Water through Nanotechnology: Needs, Gaps, and Fulfillment. *ACS Nano* **2020**, 6420.

(8) Alvarez, P. J. J.; Chan, C. K.; Elimelech, M.; Halas, N. J.; Villagrán, D. Emerging Opportunities for Nanotechnology to Enhance Water Security. *Nat. Nanotechnol.* **2018**, *13*, 634−641.

(9) Srimuk, P.; Su, X.; Yoon, J.; Aurbach, D.; Presser, V. Charge-Transfer Materials for Electrochemical Water Desalination, Ion Separation and the Recovery of Elements. *Nat. Rev. Mater.* **2020**, 517.

(10) Bibby, A.; Mercier, L. Mercury(Ii) Ion Adsorption Behavior in Thiol-Functionalized Mesoporous Silica Microspheres. *Chem. Mater.* **2002**, *14*, 1591−1597.

(11) Oh, Y.; Bag, S.; Malliakas, C. D.; Kanatzidis, M. G. Selective Surfaces: High-Surface-Area Zinc Tin Sulfide Chalcogels. *Chem. Mater.* **2011**, *23*, 2447−2456.

(12) Fedoseeva, Y. V.; Orekhov, A. S.; Chekhova, G. N.; Koroteev, V. O.; Kanygin, M. A.; Senkovskiy, B. V.; Chuvilin, A.; Pontiroli, D.; Riccò, M.; Bulusheva, L. G.; Okotrub, A. V. Single-Walled Carbon Nanotube Reactor for Redox Transformation of Mercury Dichloride. *ACS Nano* **2017**, *11*, 8643−8649.

(13) Kabiri, S.; Tran, D. N. H.; Azari, S.; Losic, D. Graphene-Diatom Silica Aerogels for Efficient Removal of Mercury Ions from Water. *ACS Appl. Mater. Interfaces* **2015**, *7*, 11815−11823.

(14) Li, B.; Zhang, Y.; Ma, D.; Shi, Z.; Ma, S. Mercury Nano-Trap for Effective and Efficient Removal of Mercury(Ii) from Aqueous Solution. *Nat. Commun.* **2014**, *5*, 5537.

(15) Yee, K.-K.; Reimer, N.; Liu, J.; Cheng, S.-Y.; Yiu, S.-M.; Weber, J.; Stock, N.; Xu, Z. Effective Mercury Sorption by Thiol-Laced Metal-Organic Frameworks: In Strong Acid and the Vapor Phase. *J. Am. Chem. Soc.* **2013**, *135*, 7795−7798.

(16) Fausey, C. L.; Zucker, I.; Lee, D. E.; Shaulsky, E.; Zimmerman, J. B.; Elimelech, M. Tunable Molybdenum Disulfide-Enabled Fiber Mats for High-Efficiency Removal of Mercury from Water. *ACS Appl. Mater. Interfaces* **2020**, *12*, 18446−18456.

(17) Yap, P. L.; Kabiri, S.; Tran, D. N. H.; Losic, D. Multifunctional Binding Chemistry on Modified Graphene Composite for Selective and Highly Efficient Adsorption of Mercury. *ACS Appl. Mater. Interfaces* **2019**, *11*, 6350−6362.

(18) Velempini, T.; Pillay, K. Sulphur Functionalized Materials for Hg(Ii) Adsorption: A Review. *J. Environ. Chem. Eng.* **2019**, *7*, 103350.

(19) Ai, K.; Ruan, C.; Shen, M.; Lu, L. Mos_2 Nanosheets with Widened Interlayer Spacing for High-Efficiency Removal of Mercury in Aquatic Systems. *Adv. Funct. Mater.* **2016**, *26*, 5542−5549.

(20) Liu, C.; Wu, T.; Hsu, P.-C.; Xie, J.; Zhao, J.; Liu, K.; Sun, J.; Xu, J.; Tang, J.; Ye, Z.; Lin, D.; Cui, Y. Direct/Alternating Current Electrochemical Method for Removing and Recovering Heavy Metal from Water Using Graphene Oxide Electrode. *ACS Nano* **2019**, *13*, 6431−6437.

(21) Chen, R.; Sheehan, T.; Ng, J. L.; Brucks, M.; Su, X. Capacitive Deionization and Electrosorption for Heavy Metal Removal. *Environ. Sci.: Water Res. Technol.* **2020**, *6*, 258−282.

(22) Su, X.; Kulik, H. J.; Jamison, T. F.; Hatton, T. A. Anion-Selective Redox Electrodes: Electrochemically Mediated Separation with Heterogeneous Organometallic Interfaces. *Adv. Funct. Mater.* **2016**, *26*, 3394−3404.

(23) Su, X.; Kushima, A.; Halliday, C.; Zhou, J.; Li, J.; Hatton, T. A. Electrochemically-Mediated Selective Capture of Heavy Metal Chromium and Arsenic Oxyanions from Water. *Nat. Commun.* **2018**, *9*, 4701.

(24) Su, X.; Tan, K.-J.; Elbert, J.; Rüttiger, C.; Gallei, M.; Jamison, T. F.; Hatton, T. A. Asymmetric Faradaic Systems for Selective Electrochemical Separations. *Energy Environ. Sci.* **2017**, *10*, 1272−1283.

(25) Su, X. Electrochemical Interfaces for Chemical and Biomolecular Separations. *Curr. Opin. Colloid Interface Sci.* **2020**, 77.

(26) Tan, K.-J.; Su, X.; Hatton, T. A. An Asymmetric Iron-Based Redox-Active System for Electrochemical Separation of Ions in Aqueous Media. *Adv. Funct. Mater.* **2020**, *30*, 1910363.

(27) Kim, K.; Cotty, S.; Elbert, J.; Chen, R.; Hou, C.-H.; Su, X. Asymmetric Redox-Polymer Interfaces for Electrochemical Reactive Separations: Synergistic Capture and Conversion of Arsenic. *Adv. Mater.* **2020**, *32*, No. e1906877.

(28) Lee, J.; Srimuk, P.; Fleischmann, S.; Su, X.; Hatton, T. A.; Presser, V. Redox-Electrolytes for Non-Flow Electrochemical Energy Storage: A Critical Review and Best Practice. *Prog. Mater. Sci.* **2019**, *101*, 46−89.

(29) Su, X.; Hatton, T. A. Redox-Electrodes for Selective Electrochemical Separations. *Adv. Colloid Interface Sci.* **2017**, *244*, 6−20.

(30) Kim, K.; Baldaguez Medina, P.; Elbert, J.; Kayiwa, E.; Cusick, R. D.; Men, Y.; Su, X. Molecular Tuning of Redox-Copolymers for Selective Electrochemical Remediation. *Adv. Funct. Mater.* **2020**, 2004635.

(31) Kim, Y.; Lin, Z.; Jeon, I.; Van Voorhis, T.; Swager, T. M. Polyaniline Nanofiber Electrodes for Reversible Capture and Release of Mercury(Ii) from Water. *J. Am. Chem. Soc.* **2018**, *140*, 14413−14420.

(32) Tunsu, C.; Wickman, B. Effective Removal of Mercury from Aqueous Streams Via Electrochemical Alloy Formation on Platinum. *Nat. Commun.* **2018**, *9*, 4876.

(33) Bernardi, M.; Giulianini, M.; Grossman, J. C. Self-Assembly and Its Impact on Interfacial Charge Transfer in Carbon Nanotube/P3ht Solar Cells. *ACS Nano* **2010**, *4*, 6599−6606.

(34) Rudolph, M.; Ratcliff, E. L. Normal and Inverted Regimes of Charge Transfer Controlled by Density of States at Polymer Electrodes. *Nat. Commun.* **2017**, *8*, 1048.

(35) Lai, C.-H.; Ashby, D. S.; Lin, T. C.; Lau, J.; Dawson, A.; Tolbert, S. H.; Dunn, B. S. Application of Poly(3-Hexylthiophene-2,5-

https://dx.doi.org/10.1021/acsami.0c15570
ACS Appl. Mater. Interfaces 2020, 12, 49713−49722

Diyl) as a Protective Coating for High Rate Cathode Materials. *Chem. Mater.* **2018**, *30*, 2589−2599.
(36) Ludwig, S. *P3ht Revisited - from Molecular Scale to Solar Cell Devices*; Springer: New York, 2014.
(37) Yu, D.; Yang, Y.; Durstock, M.; Baek, J.-B.; Dai, L. Soluble P3ht-Grafted Graphene for Efficient Bilayer-Heterojunction Photovoltaic Devices. *ACS Nano* **2010**, *4*, 5633−5640.
(38) Enengl, C.; Enengl, S.; Pluczyk, S.; Havlicek, M.; Lapkowski, M.; Neugebauer, H.; Ehrenfreund, E. Doping-Induced Absorption Bands in P3ht: Polarons and Bipolarons. *ChemPhysChem* **2016**, *17*, 3836−3844.
(39) Jenkins, J. L.; Lee, P. A.; Nebesny, K. W.; Ratcliff, E. L. Systematic Electrochemical Oxidative Doping of P3ht to Probe Interfacial Charge Transfer across Polymer−Fullerene Interfaces. *J. Mater. Chem. A* **2014**, *2*, 19221−19231.
(40) Kao, E.; Liang, Q.; Bertholet, G. R.-K.; Zang, X.; Park, H. S.; Bae, J.; Lu, J.; Lin, L. Electropolymerized Polythiophene Photoelectrodes for Photocatalytic Water Splitting and Hydrogen Production. *Sens. Actuators, A* **2018**, *277*, 18−25.
(41) Holliday, S.; Ashraf, R. S.; Wadsworth, A.; Baran, D.; Yousaf, S. A.; Nielsen, C. B.; Tan, C. H.; Dimitrov, S. D.; Shang, Z.; Gasparini, N.; Alamoudi, M.; Laquai, F.; Brabec, C. J.; Salleo, A.; Durrant, J. R.; McCulloch, I. High-Efficiency and Air-Stable P3ht-Based Polymer Solar Cells with a New Non-Fullerene Acceptor. *Nat. Commun.* **2016**, *7*, 11585.
(42) Su, X.; Hübner, J.; Kauke, M. J.; Dalbosco, L.; Thomas, J.; Gonzalez, C. C.; Zhu, E.; Franzreb, M.; Jamison, T. F.; Hatton, T. A. Redox Interfaces for Electrochemically Controlled Protein−Surface Interactions: Bioseparations and Heterogeneous Enzyme Catalysis. *Chem. Mater.* **2017**, *29*, 5702−5712.
(43) Yang, H.; Shin, T. J.; Yang, L.; Cho, K.; Ryu, C. Y.; Bao, Z. Effect of Mesoscale Crystalline Structure on the Field-Effect Mobility of Regioregular Poly(3-Hexyl Thiophene) in Thin-Film Transistors. *Adv. Funct. Mater.* **2005**, *15*, 671−676.
(44) Diao, Y.; Shaw, L.; Bao, Z.; Mannsfeld, S. C. B. Morphology Control Strategies for Solution-Processed Organic Semiconductor Thin Films. *Energy Environ. Sci.* **2014**, *7*, 2145−2159.
(45) Qu, S.; Wang, M.; Chen, Y.; Yao, Q.; Chen, L. Enhanced Thermoelectric Performance of Cnt/P3ht Composites with Low Cnt Content. *RSC Adv.* **2018**, *8*, 33855−33863.
(46) Hepler, L. G.; Olofsson, G. Mercury. Thermodynamic Properties, Chemical Equilibriums, and Standard Potentials. *Chem. Rev.* **1975**, *75*, 585−602.
(47) Modak, A.; Das, S.; Chanda, D. K.; Samanta, A.; Jana, S. Thiophene Containing Microporous and Mesoporous Nanoplates for Separation of Mercury from Aqueous Solution. *New J. Chem.* **2019**, *43*, 3341−3349.
(48) Haseen, U.; Ahmad, H. Preconcentration and Determination of Trace Hg(Ii) Using a Cellulose Nanofiber Mat Functionalized with Mos_2 Nanosheets. *Ind. Eng. Chem. Res.* **2020**, *59*, 3198−3204.
(49) Fu, Y.; Pao, T.; Chen, S.-Z.; Yau, S.; Dow, W.-P.; Lee, Y.-L. Electrodeposition of Copper on a Pt(111) Electrode in Sulfuric Acid Containing Poly(Ethylene Glycol) and Chloride Ions as Probed by in Situ Stm. *Langmuir* **2012**, *28*, 10120−10127.
(50) Wu, H. P. Nature and Stability of Mercury Thin Films on Glassy Carbon Electrodes under Fast-Scan Anodic Stripping Voltammetry. *Anal. Chem.* **1994**, *66*, 3151−3157.
(51) Grujicic, D.; Pesic, B. Electrodeposition of Copper: The Nucleation Mechanisms. *Electrochim. Acta* **2002**, *47*, 2901−2912.
(52) Emery, S. B.; Hubbley, J. L.; Roy, D. Voltammetric and Amperometric Analyses of Electrochemical Nucleation: Electrodeposition of Copper on Nickel and Tantalum. *J. Electroanal. Chem.* **2004**, *568*, 121−133.
(53) Salinas, D. R.; Cobo, E. O.; García, S. G.; Bessone, J. B. Early Stages of Mercury Electrodeposition on Hopg. *J. Electroanal. Chem.* **1999**, *470*, 120−125.
(54) Geng, J.; Kong, B.-S.; Yang, S. B.; Youn, S. C.; Park, S.; Joo, T.; Jung, H.-T. Effect of Swnt Defects on the Electron Transfer Properties in P3ht/Swnt Hybrid Materials. *Adv. Funct. Mater.* **2008**, *18*, 2659−2665.
(55) Patel, R. J.; Tighe, T. B.; Ivanov, I. N.; Hickner, M. A. Electro-Optical Properties of Electropolymerized Poly(3-Hexylthiophene)/Carbon Nanotube Composite Thin Films. *J. Polym. Sci., Part B: Polym. Phys.* **2011**, *49*, 1269−1275.
(56) Hudecz, D.; Khire, T.; Chung, H. L.; Adumeau, L.; Glavin, D.; Luke, E.; Nielsen, M. S.; Dawson, K. A.; McGrath, J. L.; Yan, Y. Ultrathin Silicon Membranes for *in Situ* Optical Analysis of Nanoparticle Translocation across a Human Blood−Brain Barrier Model. *ACS Nano* **2020**, *14*, 1111−1122.
(57) Kim, D.-H.; Jang, H.-S.; Kim, C.-D.; Cho, D.-S.; Yang, H.-S.; Kang, H.-D.; Min, B.-K.; Lee, H.-R. Dynamic Growth Rate Behavior of a Carbon Nanotube Forest Characterized by in Situ Optical Growth Monitoring. *Nano Lett.* **2003**, *3*, 863−865.
(58) Zhu, X.; Alexandratos, S. D. Determination of Trace Levels of Mercury in Aqueous Solutions by Inductively Coupled Plasma Atomic Emission Spectrometry: Elimination of the 'Memory Effect'. *Microchem. J.* **2007**, *86*, 37−41.
(59) Ratcliff, E. L.; Jenkins, J. L.; Nebesny, K.; Armstrong, N. R. Electrodeposited, "Textured" Poly(3-Hexyl-Thiophene) (E-P3ht) Films for Photovoltaic Applications. *Chem. Mater.* **2008**, *20*, 5796−5806.

https://dx.doi.org/10.1021/acsami.0c15570
ACS Appl. Mater. Interfaces 2020, 12, 49713−49722